HAL
open science

Gas-Phase Rate Coefficient of OH + 1,2-Epoxybutane Determined between 220 and 950 K

Hajar El Othmani, Yangang Ren, Yuri Bedjanian, Souad El Hajjaji, Carmen Tovar, Peter Wiesen, Abdelwahid S Mellouki, Max Mcgillen, Véronique Daële

To cite this version:

Hajar El Othmani, Yangang Ren, Yuri Bedjanian, Souad El Hajjaji, Carmen Tovar, et al.. Gas-Phase Rate Coefficient of OH + 1,2-Epoxybutane Determined between 220 and 950 K. ACS Earth and Space Chemistry, 2021, 5 (4), pp.960-968. 10.1021/acsearthspacechem.1c00050 . hal-03195480

HAL Id: hal-03195480

https://hal.science/hal-03195480v1

Submitted on 23 Sep 2021

HAL is a multi-disciplinary open access archive for the deposit and dissemination of scientific research documents, whether they are published or not. The documents may come from teaching and research institutions in France or abroad, or from public or private research centers.

L'archive ouverte pluridisciplinaire **HAL**, est destinée au dépôt et à la diffusion de documents scientifiques de niveau recherche, publiés ou non, émanant des établissements d'enseignement et de recherche français ou étrangers, des laboratoires publics ou privés.

Title:

Gas-phase rate coefficient of OH + 1,2-epoxybutane determined between 220 and 950 K

Author list:

Hajar El Othmani,[1,2] Yangang Ren,[1] Yuri Bedjanian,[1] Souad El Hajjaji,[2] Carmen Tovar,[3] Peter Wiesen,[3] Abdelwahid Mellouki,[1] Max R. McGillen,[1,*] Véronique Daële[1,*]

[1] Institut de Combustion Aérothermique Réactivité et Environnement/OSUC-CNRS, 1C Avenue de la Recherche Scientifique, 45071 Orléans Cedex 2, France

[2] Faculty of Science, Mohammed V University in Rabat, 4 Avenue Ibn Battouta, B.P. 1040,10100 Rabat, Morocco

[3] University of Wuppertal, Institute for Atmospheric & Environmental Research, D-42097 Wuppertal, Germany

*Correspondence to: Véronique Daële (veronique.daele@cnrs-orleans.fr) and Max R. McGillen (max.mcgillen@cnrs-orleans.fr)

Keywords:

Epoxide, hydroxyl, kinetics, atmospheric chemistry, non-Arrhenius

Abstract:

Epoxides have many primary and secondary atmospheric sources. As with other oxygenates, they exhibit a complex temperature-dependent reaction with OH, whose full description is necessary in order to understand their interactions in atmospheric and combustion environments. We measured the kinetics of the title reaction using two complementary absolute methods: pulsed-laser photolysis–laser-induced fluorescence (PLP–LIF) and a discharge-flow mass spectrometric system (DF-MS), both monitoring temporal decays in OH. In addition, two relative methods employing the DF-MS as a function of temperature, as well as several simulation chamber experiments at room temperature were performed. A very weak negative temperature dependence was observed at T≤285 K, and only through the combination of precise data and a large temperature range were we able to discern the transition towards positive temperature dependence found at T≥295 K. The non-Arrhenius temperature dependence of OH + 1,2-epoxybutane implies the agency of pre-reactive complexes in this reaction mechanism, albeit with a smaller effect than with its acyclic ether analogues. This will have implications for understanding the chemical fate of epoxides within oxidizing environments.

1. Introduction:

Many epoxide-forming reaction channels have so far been identified. Within the atmosphere, these may include simple association reactions with oxidants such as $O(^3P)$ + alkenes,[1] NO_3 + alkenes,[2] O_3 + conjugated dialkenes,[3–5] and O_3 + halogenated/ sterically hindered alkenes.[6] Potentially more important are the unimolecular processes such as ring-closure reactions that occur for hydroperoxyalkyl radicals,[7,8] and unsaturated hydroperoxides.[9] These have been implicated in the formation of highly functionalized oxidation products of biogenic volatile organic compounds such as isoprene epoxydiols (IEPOX), key gas-phase oxidation products of isoprene.

There are several primary emissions of epoxides relating to industrial production, e.g. alkoxylation reactions for polymer synthesis,[10] as well as natural emissions such as floral perfumes and other semiochemicals.[11]

Once epoxides enter the atmosphere, they will engage in subsequent reactions. Notable among these are acid-catalyzed ring-opening processes, which lead to highly functionalized polyol species. These products have a greatly reduced volatility compared with the epoxide starting

material, and are thought to contribute significantly to secondary organic aerosol production.[12–14] However, these multiphase processes occur in competition with gas-phase oxidation reactions in the atmosphere, the most important of which is expected to be hydrogen abstraction reactions with the OH radical. By querying a recently compiled near-comprehensive database of gas-phase atmospheric reactions of organic compounds,[15] it can be concluded that as few as two epoxides have been studied as a function of temperature: ethylene oxide and 1,2-propylene oxide.[16,17]

With such limited knowledge of the OH kinetics, the overall atmospheric fate of epoxides therefore remains highly uncertain. We address this by taking a relatively simple epoxide, 1,2-epoxybutane (EPB), and subjecting it to a set of precise and accurate kinetic measurements, such that we can better understand the effects of the epoxide functionality on chemical reactivity throughout the tropospheric temperature range and higher, which may be of importance to combustion chemistry.

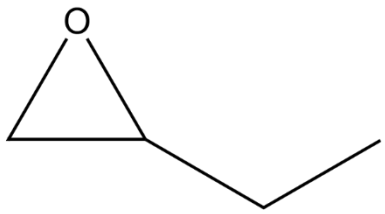

Structure of 1,2-epoxybutane (EPB)

2. Experimental methods:

2.1. Absolute measurements:

Two absolute techniques were employed in this study to measure the temperature-dependent rate coefficient of Reaction 1:

1,2-epoxybutane + OH → products Reaction 1

Notably, the pulsed-laser photolysis–laser-induced fluorescence (PLP–LIF) technique, and the discharge-flow mass spectrometry method (DF-MS), which are described in the following subsections.

2.1.1. Pulsed-Laser Photolysis–Laser-induced by fluorescence measurements:

The PLP–LIF system has been described in detail elsewhere,[17] and will be described only briefly here. This system consists of a 5-way cross Pyrex reaction cell (volume = 200 cm^3), the

gaseous contents of which were temperature-regulated by circulating heated or cooled fluid through an outer jacket. Measurements were conducted over the temperature range 220–373 K and ~100 Torr of bath gas (He), and were performed under pseudo-first-order conditions, where [EPB] >> [OH]. OH radicals were produced in Reactions 2 or 3 from OH precursors (H_2O_2 or HNO_3) that were photolyzed at 10 Hz at a wavelength of 248 nm by a KrF excimer laser pulse.

$H_2O_2 + h\nu \rightarrow 2OH$ Reaction 2

$HNO_3 + h\nu \rightarrow OH + NO_2$ Reaction 3

OH radicals were detected following excitation from a probe laser pulse, tuned to excite the $A^2\Sigma^+(\nu = 1) \leftarrow X^2\Pi\ (\nu = 0)$ transition near 282 nm using a frequency-doubled Nd:YAG pumped dye laser. The resulting fluorescence was detected using a photomultiplier tube fitted with a 308 nm bandpass filter. The photomultiplier signal was collected using a boxcar integrator and recorded on a data acquisition card (see Figure S1, Supporting Information SI). Temporal profiles of integrated OH signal were collected by changing the delay time between the photolysis and probe lasers, which, under pseudo-first-order conditions obey the following relationship:

$$\ln\left(\frac{[\mathrm{OH}]_t}{[\mathrm{OH}]_0}\right) = \ln\left(\frac{S_t}{S_0}\right) = -(k[\text{1,2-epoxybutane}] + k_d)t = -k't \qquad \text{Equation 1}$$

where t is the delay time between laser pulses, S is the OH fluorescence signal, integrated over the box-car sampling window, and k' and k_d represent the pseudo-first-order decay rate of OH in the presence or absence of EPB respectively. Values of k_d were typically 30–150 s^{-1} and were a consequence of the reaction of OH with the OH precursor (H_2O_2 or HNO_3) and diffusion of OH out of the reaction volume. We expect that this diffusion term is not truly first-order in nature, and besides, given that signal:noise is reduced at long delay times, in order to ensure high-quality first-order fits in each case, we limited our temporal profiles to include only the first three decades of integrated OH fluorescence signal. Values for k' were obtained through an error-weighted least-squares fit of S_t vs t. Following this, an error-weighted least-squares fit of k' against [EPB] yielded a slope equal to the bimolecular rate coefficient, k. This procedure was conducted at each temperature of the dataset.

As with similar studies,[20,21] in order to reduce systematic uncertainties in this relationship, EPB concentrations were quantified on-line using a multipass Fourier transform infrared spectrometer (pathlength = 1000 cm). For this purpose, the infrared band intensity of EPB was determined. This was achieved by introducing known concentrations of EPB from a manometrically prepared sample bulb (He bath gas) into the multipass cell, and the absorbance was quantified over a range of concentrations. Absorbance was found to obey the Beer-Lambert

law over the concentration range of our measurement. During experiments, [EPB] was monitored on-line, whereby the FTIR absorption cell was situated directly downstream from the LIF reactor. Figure S2 shows a plot of the integrated band intensity determination.

2.1.2. Discharge-flow mass spectrometry measurements:

Complementary measurements were performed using a fast-flow reactor coupled with a molecular beam sampling electron impact ionization quadrupole mass spectrometer.[22,23] These measurements were performed over a pressure range of 2–9 Torr (He), and were conducted in one of two reactors, either for low- or high-temperature measurements. The low-temperature flow reactor covered the temperature range 240–340 K, and consisted of a Pyrex tube (45 cm in length, 2.4 cm i.d.) with an outer jacket through which a temperature-regulated fluid was circulated (see Figure S3). To minimize wall-loss of OH, the inner surface of the reactor, as well as the movable injector, were coated with halocarbon wax. The high-temperature flow reactor was employed over the temperature range 360–950 K, a quartz tube (45 cm in length, 2.5 cm i.d.), where the temperature was controlled with electrical heating elements (see Figure S4).

OH was produced by passing H_2 in a bath gas (He) through a microwave discharge, yielding H atoms, which subsequently react with NO_2 in Reaction 4, to produce OH:

$$H + NO_2 \rightarrow OH + NO \qquad \text{Reaction 4}$$

OH radicals were detected indirectly by scavenging with Br_2, yielding HOBr (see Reaction 5), and detected at m/z 96/98 ($HOBr^+$):

$$OH + Br_2 \rightarrow HOBr + Br \qquad \text{Reaction 5}$$

The excess concentrations of Br_2 employed (3–5 × 10^{13} molecule cm^{-3}) combined with the rapidity of Reaction 4, leads to efficient scavenging under our experimental conditions. This reaction was also used to determine absolute concentrations of OH through their chemical conversion to HOBr in an excess of Br_2, whereby [OH] = [HOBr] = $\Delta[Br_2]$, i.e. the concentration of OH (HOBr) was determined from the consumed fraction of $[Br_2]$. A detailed discussion on the possible influence of secondary chemistry on this method of OH detection and determination of the absolute concentrations of the radicals is presented elsewhere.[24]

EPB was delivered to the reactor by passing carrier gas (He) over a liquid sample of pure EPB, and was detected by mass spectrometry at its parent ion of m/z = 72 ($C_4H_8O^+$). The absolute

calibration of the mass spectrometer for EPB was performed by two methods. Firstly, absolute concentrations of EPB (as well as of other stable species, NO_2, Br_2 and *n*-butane) were calculated from the flow rates obtained from the measurements of the pressure drop of the manometrically prepared mixtures in He stored in calibrated volume flasks. Secondly, a known volume (generally, 0.6 µl) of sample was injected into a helium flow in the reactor under the experimental conditions of the kinetic measurements (pressure, temperature, total flow of bath gas) and the mass peak at $m/z = 72$ was recorded. The integrated area of the mass spectrometric signal, corresponding to the total number of EPB molecules injected into the reactor, allowed the determination of the calibration factor. These two methods were found to agree within 10%.

2.2. Relative rate measurements:

In addition to the absolute measurements of Section 2.1., two relative rate techniques were used to determine the rate coefficient of Reaction 1, notably, the same DF-MS described earlier to make temperature-dependent measurements, but operated in a different mode; and a 7.3 m^3 Teflon atmospheric simulation chamber, used to make room-temperature measurements. These are described in the following subsections.

2.2.1. Discharge-flow mass spectrometry:

The DF-MS was used to determine the decay rate of EPB in the presence of a reference compound (Reaction 6), whose rate coefficient is already known:

Reference + OH → products Reaction 6

Comparing these decay rates, the rate coefficient is determined from the following equation:

$$\ln\left(\frac{[\text{1,2-epoxybutane}]_0}{[\text{1,2-epoxybutane}]_t}\right) = \frac{k_{\text{1,2-epoxybutane}}}{k_{\text{reference}}}\ln\left(\frac{[\text{reference}]_0}{[\text{reference}]_t}\right) \qquad \text{Equation 2}$$

where subscripts 0 and *t* refer to initial species concentrations at time 0 and time *t* respectively. In this case, the reference compound was *n*-butane, which has a well characterized temperature dependence over a large temperature range (231–1236 K).[15]

$$k(T) = 2.09 \times 10^{-12}\exp\left(\frac{42}{T}\right)\left(\frac{T}{300}\right)^{1.82} \qquad \text{Equation 3}$$

Initial concentrations of EPB and *n*-butane were in the range 1.8–3.6 and 0.9–2.0 × 10^{12} molecule cm^{-3}, respectively. OH radicals were produced by Reaction (3) with $[NO_2] \approx 5\times10^{13}$ molecule cm^{-3}. EPB and *n*-butane were monitored by mass spectrometry at their parent peaks

at m/z = 72 and 58, respectively. A small contribution (3–4%) of EPB at m/z = 58 was observed and was subtracted from the *n*-butane signal. In addition, an appearance of a small signal at m/z = 72 (probably, as a result of *n*-butane secondary chemistry) was observed upon consumption of *n*-butane in its reaction with OH. The corresponding corrections applied to the EPB signal at m/z = 72 depended on the consumed fraction of *n*-butane and were ≤20%. Although the possible impact of secondary reactions of EPB and *n*-butane with organic radicals produced in Reactions (1) and OH + *n*-butane was not verified, it is expected to be insignificant, considering the relatively low initial concentrations of EPB and *n*-butane used in the experiments. The observed independence of the experimental results of the reaction time, which was varied from 0.02 to 0.04 s, and their good agreement (within the region of overlap) with the data obtained for the other methods of this study supports this assumption. Another possible secondary loss of EPB/ *n*-butane may be initiated by oxygen atoms formed in the self-reaction of OH radicals (see Reaction 7):

$$OH + OH \rightarrow O + H_2O \qquad \text{Reaction 7}$$

whose rate coefficient is as follows:

$$k_7 = 2.68\times10^{-14}\times(T/300)^{2.75}\exp(1165/T)\ \text{cm}^3\text{molecule}^{-1}\text{s}^{-1}\ (T=220–2384\ \text{K}),^{25} \qquad \text{Equation 4}$$

but this has a negligible effect on the concentrations of EPB and *n*-butane, because O-atoms are mainly consumed in the rapid reactions with OH radicals and NO_2 present in high concentrations in the reactor:

$$O + NO_2 \rightarrow NO + O_2 \qquad \text{Reaction 8}$$

$$k_8 = 6.1\times10^{-12}\exp(155/T)\ \text{cm}^3\ \text{molecule}^{-1}\ \text{s}^{-1}\ (T = 220–950\ \text{K}),^{26} \qquad \text{Equation 5}$$

$$O + OH \rightarrow H + O_2 \qquad \text{Reaction 9}$$

$$k_9 = 1.8\times10^{-11}\exp(180/T)\ \text{cm}^3\ \text{molecule}^{-1}\ \text{s}^{-1}\ (T = 136–515\ \text{K}),^{27} \qquad \text{Equation 6}$$

Examples of the observed plots of $\ln([\text{EPB}]_0/[\text{EPB}]_t)$ against $\ln([n\text{-butane}]_0/[n\text{-butane}]_t)$ are presented in Figure 3.

Relative rate measurements were also performed using Br_2 (Reaction 5) as a reference, conducted at a total pressure of 2–9 Torr and relied on determining the HOBr yield as a function of the $[\text{EPB}]/[Br_2]$ ratio upon OH consumption in reaction with a mixture of Br_2 and EPB.

The fraction of the initial concentration of OH radicals, $[OH]_0$, transformed to HOBr in Reaction 5, is:

$$[\mathrm{HOBr}] = \frac{k_5[\mathrm{Br_2}]}{k_5[\mathrm{Br_2}]+k_1[\mathrm{EPB}]+k_w} \times [\mathrm{OH}]_0 \qquad \text{Equation 7}$$

After rearrangement of this expression we obtain:

$$\frac{[\mathrm{OH}]_0}{[\mathrm{HOBr}]} - 1 = \frac{k_1[\mathrm{EPB}]}{k_5[\mathrm{Br_2}]} + \frac{k_w}{k_5[\mathrm{Br_2}]} \qquad \text{Equation 8}$$

At a constant concentration of Br_2, the second term in Equation 8 is constant and k_1/k_5 can be determined as the slope of the linear dependence of ($[OH]_0$/[HOBr] – 1) with [EPB]/[Br_2]. In these experiments, HOBr was monitored in both EPB-free system, corresponding to $[OH]_0$, and in the Br_2- and EPB-containing systems, corresponding to the fraction of $[OH]_0$ reacted with Br_2. Reaction time was 0.03–0.07 s, $[OH]_0$ = 2.5–6.0×10^{11} molecule cm^{-3}, concentrations of EPB and Br_2 are shown in (Table S3, SI).

2.2.2. Atmospheric simulation chamber

Relative rate measurements were also performed in the ICARE-CNRS chamber in 760 Torr of zero air bath gas at a temperature of 291±2 K. This chamber is 7.3 m^3 in volume and has been described in detail in an earlier work,[28] and has been employed in several recent studies from our group.[29,30] The walls of the chamber are constructed of FEP Teflon foil and contains two Teflon fans to ensure that the chamber contents are well mixed. In these experiments, the chamber was illuminated at 365 nm using an array of 24 × UV-A T-40 L, Viber-Lourmat lamps, to generate OH through the following sequence of reactions:

$$CH_3ONO + h\nu \rightarrow CH_3O + NO \qquad \text{Reaction 10}$$

$$CH_3O + O_2 \rightarrow HCHO + HO_2 \qquad \text{Reaction 11}$$

$$HO_2 + NO \rightarrow OH + NO_2 \qquad \text{Reaction 12}$$

In order to prevent the ingress of atmospheric contamination into the chamber through the permeability of the Teflon foil and any small leaks, experiments were performed at a slight overpressure using a continuous flow of zero air. As a consequence, chamber contents were gradually diluted over time. This was accounted for by monitoring an inert tracer (SF_6), whose concentration was determined at regular intervals, using a multipass in-situ Fourier transform infrared spectrometer. Samples of reactants were introduced into the chamber through the

injection of known volumes of liquid samples introduced into a stream of zero air flowing through a Pyrex impinger.

In these experiments, the relative rate was determined using the following equation:

$$\ln\left(\frac{[\text{1,2-epoxybutane}]_0}{[\text{1,2-epoxybutane}]_t}\right) - k_d t = \frac{k_{\text{1,2-epoxybutane}}}{k_{\text{reference}}} \ln\left(\frac{[\text{reference}]_0}{[\text{reference}]_t}\right) - k_d t \qquad \text{Equation 9}$$

which is similar to Equation 2, except that additional loss processes besides the reaction with OH (e.g. dilution, wall-loss and decomposition) are taken into account using the first-order term k_d. Two reference compounds were selected for these experiments: 2-propanol and ethanol, and these, together with the EPB were monitored continuously using a PTR-ToF-MS 8000 (Ionicon Analytik) operated in NH_4^+,[31] and H_3O^+ modes. Both 2-propanol and ethanol have well-defined OH rate coefficients at 291 K, 5.32 and 3.31 × 10^{-12} cm^3 $molecule^{-1}$ s^{-1}, respectively.[15]

2.3 Materials:

For DF-MS experiments: the purities of the gases used were as follows: He (>99.9995%, Alphagaz), passed through a liquid nitrogen trap; H_2 (>99.998%, Alphagaz); Br_2 (>99.99%, Aldrich); NO_2 (>99%, Alphagaz), EPB (>98%, Aldrich), *n*-butane (>99.5%, Air Liquide). For PLP–LIF experiments: He carrier gas (Alphagaz, 99.999%) was taken directly from the cylinder without further purification. Hydrogen peroxide, H_2O_2, (50 wt%, Aldrich) was purified over the course of several days by bubbling with zero air. Gas-phase nitric acid was taken from the headspace of a sample of 70% redistilled nitric acid, which had been dehydrated through the dropwise addition of pure H_2SO_4 added in a 1:2 ratio. Methyl nitrite was synthesized through the dropwise addition of 50% H_2SO_4 into a continuously stirred saturated solution of $NaNO_2$ in methanol maintained at 0°C, the effluent of which was swept through a water bubbler and a u-tube containing P_2O_5 using a slow flow of pure nitrogen, and trapped in a liquid nitrogen cold trap. For the atmospheric simulation chamber, ethanol (>99%, Aldrich) and 2-propanol (>99%, Aldrich) were used as references.

3. Results:

3.1. Absolute measurements:

3.1.1. PLP–LIF measurements:

Absolute overall rate coefficients were determined at temperatures between 243 and 371 K and at pressures of ~100 Torr (He). Concentrations of EPB ranged from 0.33 to 16.6 × 10^{15} molecule cm^{-3}. Initial OH concentrations, $[OH]_0$, varied from 2 to 50 × 10^{10} molecule cm^{-3}. A summary

of results together with experimental conditions are given in Table S1. Typical examples of second-order plots of k' vs [EPB] are shown in Figure 1. Under the pseudo-first-order conditions of our study, single exponential decays of OH were observed in all cases, with low scatter indicating no apparent complications of secondary chemistry or OH recycling. Second-order plots displayed good linearity in all cases, indicating that [EPB] was determined precisely and that no apparent heterogeneous or dimerization processes were perturbing the mixing ratio or reactivity of the reaction mixture.

Combined uncertainties of rate coefficients were estimated to be <10%, accounting for statistical error in k' (~3%), EPB infrared cross section (5%), pressure (2%), temperature (2%).

3.1.2. DF-MS measurements:

Absolute rate coefficients were measured over a temperature range of 298–720 K at pressures between 2.0 and 2.2 Torr (He). [EPB] was varied between 0.5 and 20 × 10^{13} molecule cm^{-3}. $[OH]_0$ ranged from 2–4 × 10^{11} molecule cm^{-3}. As with the PLP–LIF measurements, high quality single exponential decays were observed in all cases, examples of which are shown in Figure S5. All the pseudo-first order rate constants were corrected for axial and radial diffusion of OH radicals[32] with the diffusion coefficient of OH in He calculated as $D_0 = 660 \times (T/298)^{1.85}$ Torr cm^{-2} s^{-1},[33] which accounted for <11% of the observed k' values. These data are tabulated in Table S2.

Second-order plots obtained using the DF-MS method are shown in Figure 2. The y-intercepts in Figure 2 arise from wall-loss processes, k_w, are 10±5 s^{-1} over the temperature range 480 to 720 K. At 320 K, this value rises to 34±4 s^{-1}, which we attribute to surface contamination with EPB or its oxidation products. Enhanced wall-losses were observed for both halocarbon wax-coated (T < 298 K) and uncoated quartz reactors (T < 430 K), and for this reason, these temperatures were used as lower temperature limits for these respective reactors in the absolute measurements of k_1. Conversely, at temperatures >720 K, some evidence of thermal decomposition of EPB is observed in the appearance of signals at m/z = 94/96 and 108/110 which can be assigned to CH_3Br, C_2H_5Br, or fragments of potentially higher-mass products, and which could affect the absolute kinetic determinations, and was therefore considered to be an upper temperature limit for the absolute measurements of this study.

Combined uncertainties of rate coefficient determinations were estimated to be <15%, accounting for statistical error (≤5%), determination of [EPB] (~10%), mass flow (3%), pressure (2%) and temperature (1%).

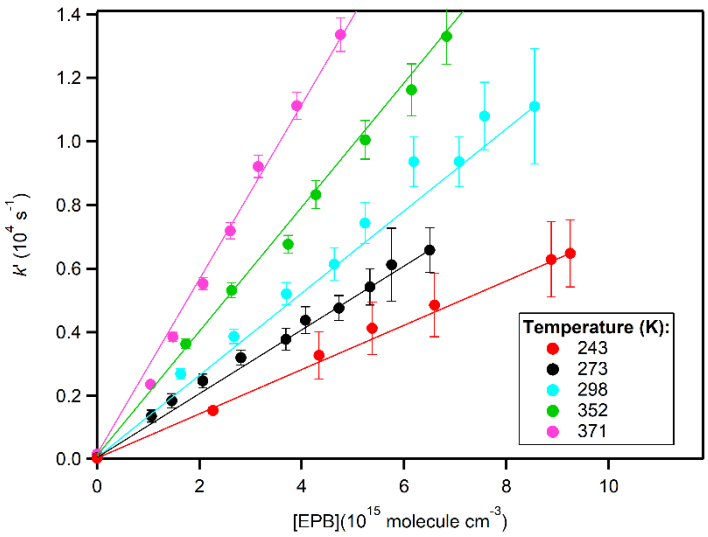

Figure 1. Dependence of the pseudo-first-order rate constant (k') on [1,2-epoxybutane] at different temperatures obtained in PLP–LIF system. Error bars represent 2σ statistical uncertainties.

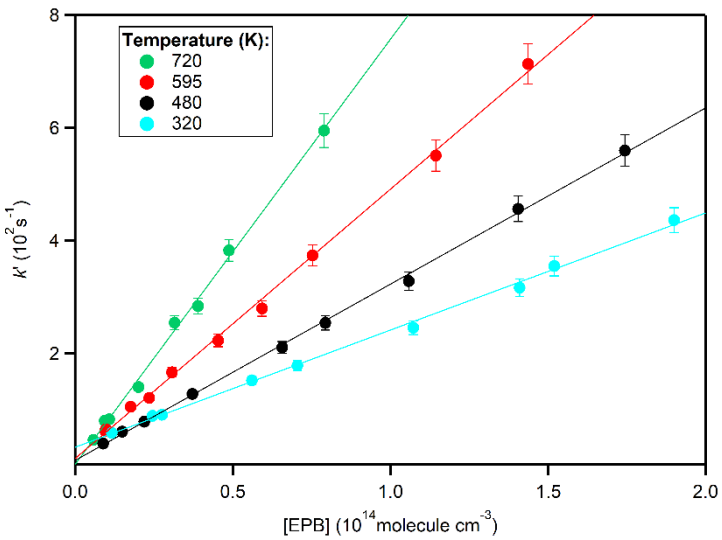

Figure 2. Pseudo-first-order rate constant (k_1') as a function of [1,2-epoxybutane] at different temperatures obtained in the DF-MS system. Partially shown error bars represent typical uncertainties (≤5%) on the determination of k_1'.

3.2. Relative rate measurements:

3.2.1. DF-MS measurements:

In order to extend the temperature range of the measurements of k_1, we used the DF-MS apparatus to make relative rate measurements, using both *n*-butane and Br_2 as reference compounds. Total pressures in the flow-tube ranged from 2–9 Torr (He). In the case of *n*-butane, rate coefficients were determined at temperatures between 275 and 950 K, and for Br_2, between 240 and 810 K. Linear relative rate plots were observed in each case, some examples of which are shown in Figures 3 and 4.

Final values of k_1, calculated using experimentally determined k_1/k_{ref} ratios. See Table S3 for tabulated data of measurements with the Br_2 reference and Table S4 for the *n*-butane reference.

The temperature dependence of OH + *n*-butane and OH + Br_2 are both well-established over the temperature range of these measurements.[15,22] Therefore, we estimate ~15% combined uncertainty in the DF-MS relative rate measurements, accounting for ~10% uncertainty in the reference rate coefficients, combined with uncertainties in temperature (1%) and statistical uncertainty in the relative rate, EPB/reference decomposition and heterogeneous loss (<5%).

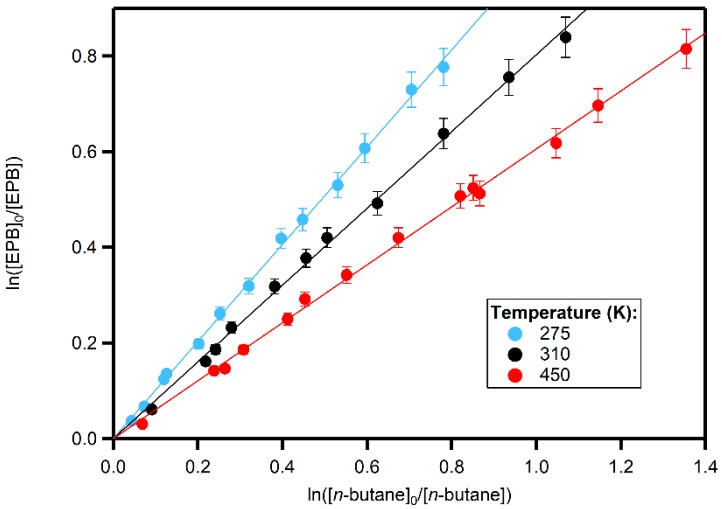

Figure 3. Relative rate plot showing the linear dependence of ln([EPB]$_0$/[EPB]) with ln(*n*-butane]$_0$/[*n*-butane]) observed at T = 275, 310 and 450 K. Error bars represent the statistical errors (<5%) in the relative rate.

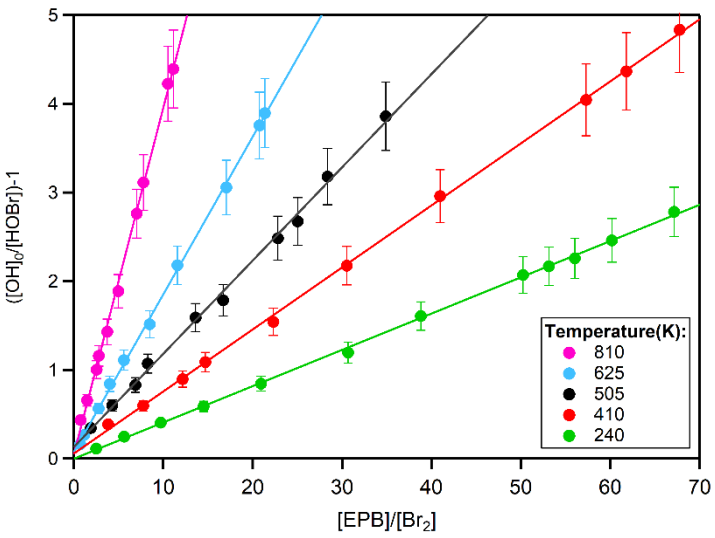

Figure 4. An alternative relative rate approach, monitoring the yield of HOBr from OH-radical titration with Br_2 + 1,2-epoxybutane mixtures at different temperatures. Error bars represent typical uncertainties of the measurements (<10%).

3.2.2. Atmospheric simulation chamber measurements:

As a further test, and to reduce the potential effects of wall interactions, a series of experiments was conducted in a 7.3 m^3 simulation chamber at 760 Torr of zero air and a temperature of 291±2K. Relative rate plots were found to be linear, with intercepts close to the origin in all cases (see Figure 5). Relative rates measured with both 2-propanol and ethanol as reference compounds were found to be in excellent agreement (1.70±0.14) and (1.71±0.11) $\times 10^{-12}$ cm^3 $molecule^{-1}$ s^{-1}, respectively, leading to a weighted-average value of (1.70±0.12) $\times 10^{-12}$ cm^3 $molecule^{-1}$ s^{-1}. These data are tabulated in Table S5.

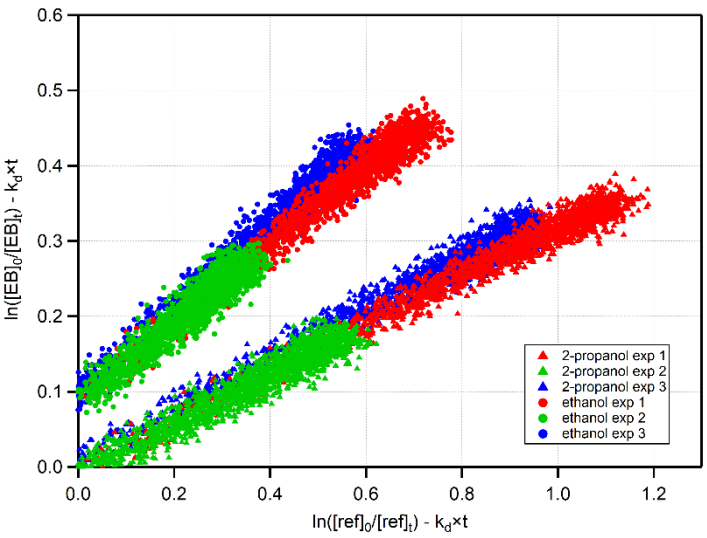

Figure 5. Plots of relative kinetic data obtained from the reaction of 1,2-epoxybutane + OH using ethanol and 2-propanol as the reference compounds. For clarity, ethanol experiments have been offset by 0.1.

4. Discussion:

All the kinetic measurements of this study are shown in Figure 6, together with the sole literature room-temperature measurement of which we are aware.[34] All measurements of this study – within their respective overlap regions – were found to be in close agreement, and were also found to agree with the literature relative rate determination. The curvature observed in the data was fitted using the following modified Arrhenius expression, and is valid over the temperature range 220–950 K:

$$k_1 = 1.72 \times 10^{-14} \times \exp\,(1407/T)(T/300)^{4.8}\ \text{cm}^3\ \text{molecule}^{-1}\ \text{s}^{-1} \qquad \text{Equation 10}$$

From Figure 6, it is apparent that the reaction of OH with EPB demonstrates clear non-Arrhenius behaviour. Indeed, this appears to be a general rule for oxygenates, wherever precise kinetic information is available over an extensive temperature range.[35] The main explanation for this phenomenon is the formation of cyclic hydrogen-bonded van der Waals (vdW) complexes, otherwise referred to as pre-reactive complexes. These structures can be stabilized into potential energy wells of ~5–33 kJ mol^{-1} for alcohols, ethers, aldehydes, ketones, esters and carboxylic acids.[36,37] The general mechanism by which vdW complexes increase the rate coefficient can be rationalized by the prolonged contact time between OH and the oxygenated co-reactant, which is afforded by stabilization into the pre-reactive complex energy well, and

which therefore provides a greater probability for quantum tunnelling processes to occur. There are several factors that determine the magnitude of this effect as a function of temperature. This relates to the binding energy of the vdW complex, which limits the lifetime of a complex at a given temperature. For strongly bound vdW complexes such as those between OH and carboxylic acids,[37] a dominantly negative temperature dependence can be observed even at 575 K for the reaction of OH with acetic acid.[38] In contrast, for weakly bound vdW complexes, such as those between OH and ketones, the onset at which a negative temperature dependence is observed in the Arrhenius diagram can be at much lower temperatures. Another aspect that can affect the tunnelling process is the entropic cost of forming the vdW. It has been observed, for example, that several vdW complexes can form for the reactions of larger species such as *n*-butanol + OH, and where it can be seen that even though the geometry may be favourable for larger cyclic vdW structures, the entropic cost of shutting down more free rotors within a molecule will reduce the overall favourability of forming the vdW complex. This results in the C–H bonds that are directly adjacent to the alcohol substitution being more reactive despite possessing a larger ring-strain associated with the 5-membered ring structure,[39] an observation that has been borne out by experimental kinetic[20] and product studies.[40] A further factor affecting the importance of vdW complexes is the width of the barrier going towards products, whereby quantum tunnelling becomes less probable in the case of broader barriers. This has been demonstrated experimentally by the pronounced preference of hydrogen abstraction from the O–H bond in methanol at very low temperatures, which involves traversing a high (yet narrow) barrier towards forming the methoxy radical + H_2O.[41] On a related theme, the overall bond-strength of a given reactive site may also play a role in the reactivity of a given C–H bond. In the case of 2-butanol, for example, the alpha tertiary hydrogen atom is especially weak (92.9 kcal/mol),[42,43] which is estimated to account for 63% of the overall reactivity of the molecule at room temperature.[20] In contrast, the reactivity of the two alpha secondary hydrogen atoms in *n*-butanol are slightly stronger (93.2 kcal/mol),[42,43] and only account for 28% of the total room temperature rate coefficient on a per hydrogen basis.[20]

However, it is acknowledged that negative temperature dependence has been observed experimentally in several other metathesis reactions, notably those of alkyl radicals with hydrogen halides.[44] Subsequently, this temperature-dependent behaviour was rationalized through a modified transition state theory (MTST), which, when applied to systems with negative apparent activation energies, can explain negative temperature dependence without invoking statistical intermediate complexes.[45] Furthermore MTST predicts the transition from

negative to positive temperature dependence in several reactions, similar to that observed in our case for OH + EPB.[45,46]

The EPB measurements of this study represent the first measurements of the reaction of an epoxide with OH over an extended temperature range. To provide a context for what we observe, we show in Figure 7 an Arrhenius diagram of several other molecules, each of which have been measured over an extended temperature range, and like EPB, possess 8 C–H bonds.[15] When the temperature dependence is compared with that of what we could take to be a base case alkane-like reactivity of OH + propane, it becomes apparent that the epoxide functionality does not impart a strong increase in the overall reactivity of this molecule. This contrasts markedly with acyclic ethers such as methyl ethyl ether, which is significantly more reactive than propane across the entire temperature range. An even more potent effect is observed for the reaction of *n*-butanal, which can at least in part be explained by the relative weakness of the aldehydic C–H bond. Conversely, the temperature dependence of EPB appears to be somewhere intermediate between the alcohols and alkanes. As explained above, there are several potential reasons for this. We note that the C–H bonds are relatively strong directly adjacent to the epoxide ring: 102 and 103 kcal/mol for the tertiary and secondary sites respectively, and the most favourable reaction site is probably the remaining secondary C–H bonds, which possess a BDE of 95.9 kcal/mol.[42,43] Assuming this to be the case and that the curvature that is observed is indeed associated with the formation of a vdW complex, we can hypothesize that such a configuration would lead to a bicylic structure such as this:

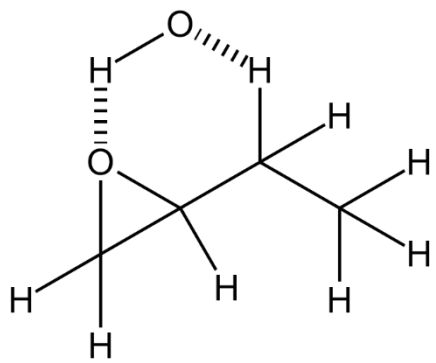

which would restrict the rotation of the epoxide group, the formation of which is entropically costly and becomes favourable only at low temperatures. We expect that detailed theoretical calculations would be useful in constraining this mechanism further; however, this is outside the scope of the present study. In addition, it would be valuable to obtain quantitative product yield data, especially as a function of temperature, since it has been demonstrated in some oxygenated systems such as *i*-butanol, that a relatively temperature independent region of the

Arrhenius diagram can be underlain by several more temperature-dependent reaction channels offsetting each other.[47]

With regards to the atmospheric implications of epoxide chemistry, based on the EPB + OH kinetics, it would appear that the epoxide functionality does not enhance reactivity strongly in the tropospheric temperature range, and simple epoxides such as this may react at similar rates to alkanes. For more functionalized epoxides such as the IEPOX derivatives, larger rate coefficients are observed, which is likely to relate to the enhanced reactivity of the functional groups to which the epoxide moiety is attached.[48,49] It is therefore probable that for simple epoxides and those epoxides that possess deactivating functional groups such as ketones, that acid-catalyzed ring-opening becomes highly competitive with oxidative loss under tropospheric conditions. Conversely, for more functionalized epoxides, reaction with OH may represent an important sink.

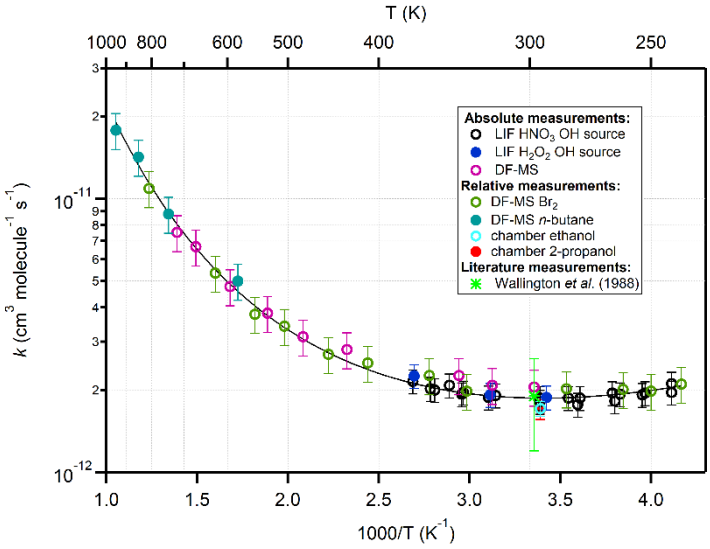

Figure 6. Summary of the OH + 1,2-epoxybutane rate coefficients obtained in this work, together with the sole room-temperature literature determination. The line represents an error-weighted fit to all data (see Equation 10). Error bars represent the total combined uncertainties for each determination (see Results section).

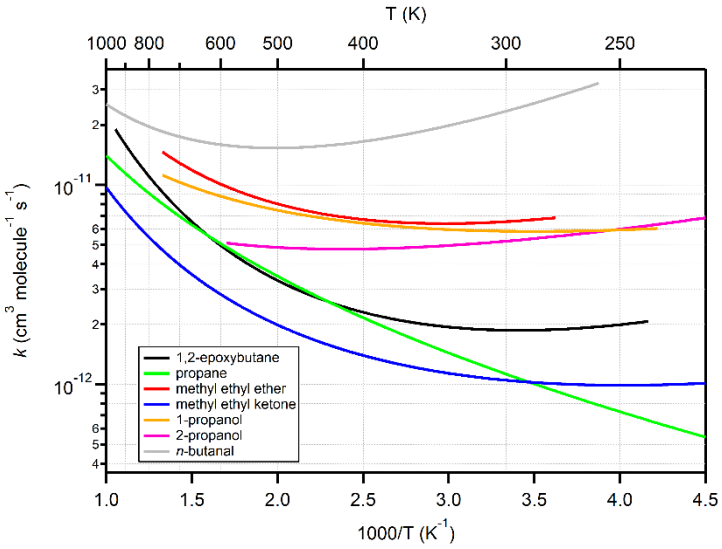

Figure 7. Arrhenius diagram comparing the temperature dependence of the OH + 1,2-epoxybutane rate coefficient with analogous molecules possessing 8 C–H bonds taken from a recently compile kinetic database.[15]

5. Conclusions:

Absolute and relative measurements of the rate coefficient of 1,2-epoxybutane + OH have been determined over a temperature range between 220 and 950 K. Excellent agreement between these measurements and techniques was observed in their respective regions of overlap. The high precision of the measurements combined with the large temperature range allows us to observe the non-Arrhenius behaviour of this rate coefficient. This represents the first epoxide whose rate coefficient has been measured over an extended temperature range, which provides new insights into the reactivity of the epoxide functional group. Curvature is observed at the lower temperatures of this study, which suggests that van der Waals complexes are playing a role in the reaction mechanism within the tropospheric temperature range. The data obtained for this simple epoxide suggests that the epoxide moiety itself is not especially reactive, and that the fate of more functionalized epoxides with respect to bimolecular processes in the atmosphere is likely to be governed by the reactivity of functional groups to which the epoxide is attached. Detailed theoretical calculations and quantitative product yield studies would be useful in understanding the reaction mechanism further.

Acknowledgments

This work is supported by Labex Voltaire (ANR-10-LABX-100-01) and the European Union's Horizon 2020 research and innovation programme through the EUROCHAMP-2020 Infrastructure Activity under grant agreement No. 730997 and the Marie Skłodowska Curie

Actions Programme (690958-MARSU-RISE-2015). MRM thanks Le Studium for their support over the duration of this project.

Reference:

(1) Cvetanović, R. J. Molecular Rearrangements in the Reactions of Oxygen Atoms with Olefins. *Can. J. Chem.* **1958**, *36* (4), 623–634. https://doi.org/10.1139/v58-088.

(2) Skov, H.; Benter, Th.; Schindler, R. N.; Hjorth, J.; Restelli, G. Epoxide Formation in the Reactions of the Nitrate Radical with 2,3-Dimethyl-2-Butene, *Cis*- and *Trans*-2-Butene and Isoprene. *Atmos. Environ.* **1994**, *28* (9), 1583–1592. https://doi.org/10.1016/1352-2310(94)90304-2.

(3) Atkinson, R.; Aschmann, S. M.; Arey, J.; Tuazon, E. C. Formation Yields of Epoxides and $O(^3P)$ Atoms from the Gas-Phase Reactions of O_3 with a Series of Alkenes. *Int. J. Chem. Kinet.* **1994**, *26* (9), 945–950. https://doi.org/10.1002/kin.550260908.

(4) Santos, C. dos; de Rosso, C. R. S.; Imamura, P. M. Synthesis Of New Chiral Synthons Through Regioselective Ozonolysis Of Methyl Abietate. *Synth. Commun.* **1999**, *29* (11), 1903–1910. https://doi.org/10.1080/00397919908086178.

(5) Atkinson, R.; Arey, J.; Aschmann, S. M.; Tuazon, E. C. Formation of $O(^3P)$ Atoms and Epoxides from the Gas- Phase Reaction of O_3 with Isoprene. *Res. Chem. Intermed.* **1994**, *20* (3–5), 385–394. https://doi.org/10.1163/156856794X00388.

(6) Bailey, P.S. *Ozonation in Organic Chemistry*; Elsevier, 1978. https://doi.org/10.1016/B978-0-12-073101-5.X5001-X.

(7) D'Ambro, E. L.; Møller, K. H.; Lopez-Hilfiker, F. D.; Schobesberger, S.; Liu, J.; Shilling, J. E.; Lee, B. H.; Kjaergaard, H. G.; Thornton, J. A. Isomerization of Second-Generation Isoprene Peroxy Radicals: Epoxide Formation and Implications for Secondary Organic Aerosol Yields. *Environ. Sci. Technol.* **2017**, *51* (9), 4978–4987. https://doi.org/10.1021/acs.est.7b00460.

(8) Møller, K. H.; Kurtén, T.; Bates, K. H.; Thornton, J. A.; Kjaergaard, H. G. Thermalized Epoxide Formation in the Atmosphere. *J. Phys. Chem. A* **2019**, *123* (49), 10620–10630. https://doi.org/10.1021/acs.jpca.9b09364.

(9) Paulot, F.; Crounse, J. D.; Kjaergaard, H. G.; Kurten, A.; St. Clair, J. M.; Seinfeld, J. H.; Wennberg, P. O. Unexpected Epoxide Formation in the Gas-Phase Photooxidation of Isoprene. *Science* **2009**, *325* (5941), 730–733. https://doi.org/10.1126/science.1172910.

(10) Brereton, G.; Emanuel, R. M.; Lomax, R.; Pennington, K.; Ryan, T.; Tebbe, H.; Timm, M.; Ware, P.; Winkler, K.; Yuan, T.; Zhu, Z.; Adam, N.; Avar, G.; Blankenheim, H.; Friederichs, W.; Giersig, M.; Weigand, E.; Halfmann, M.; Wittbecker, F.-W.; Larimer, D.-R.; Maier, U.; Meyer-Ahrens, S.; Noble, K.-L.; Wussow, H.-G. Polyurethanes. In *Ullmann's Encyclopedia of Industrial Chemistry*; Wiley-VCH Verlag GmbH & Co. KGaA: Weinheim, Germany, 2019; pp 1–76. https://doi.org/10.1002/14356007.a21_665.pub3.

(11) Brandt, K.; Dötterl, S.; Fuchs, R.; Navarro, D. M. do A. F.; Machado, I. C. S.; Dobler, D.; Reiser, O.; Ayasse, M.; Milet-Pinheiro, P. Subtle Chemical Variations with Strong Ecological Significance: Stereoselective Responses of Male Orchid Bees to Stereoisomers of Carvone Epoxide. *J. Chem. Ecol.* **2019**, *45* (5–6), 464–473. https://doi.org/10.1007/s10886-019-01072-6.

(12) Minerath, E. C.; Schultz, M. P.; Elrod, M. J. Kinetics of the Reactions of Isoprene-Derived Epoxides in Model Tropospheric Aerosol Solutions. *Environ. Sci. Technol.* **2009**, *43* (21), 8133–8139. https://doi.org/10.1021/es902304p.
(13) Minerath, E. C.; Elrod, M. J. Assessing the Potential for Diol and Hydroxy Sulfate Ester Formation from the Reaction of Epoxides in Tropospheric Aerosols. *Environ. Sci. Technol.* **2009**, *43* (5), 1386–1392. https://doi.org/10.1021/es8029076.
(14) Eddingsaas, N. C.; VanderVelde, D. G.; Wennberg, P. O. Kinetics and Products of the Acid-Catalyzed Ring-Opening of Atmospherically Relevant Butyl Epoxy Alcohols. *J. Phys. Chem. A* **2010**, *114* (31), 8106–8113. https://doi.org/10.1021/jp103907c.
(15) McGillen, M. R.; Carter, W. P. L.; Mellouki, A.; Orlando, J. J.; Picquet-Varrault, B.; Wallington, T. J. Database for the Kinetics of the Gas-Phase Atmospheric Reactions of Organic Compounds. *Earth Syst. Sci. Data* **2020**, *12* (2), 1203–1216. https://doi.org/10.5194/essd-12-1203-2020.
(16) Fritz, B.; Lorenz, K.; Steinert, W.; Zellner, R. Laboratory Kinetic Investigations of the Tropospheric Oxidation of Selected Industrial Emissions. In *Physico-Chemical Behaviour of Atmospheric Pollutants*; Versino, B., Ott, H., Eds.; Springer Netherlands: Dordrecht, 1982; pp 192–202. https://doi.org/10.1007/978-94-009-7746-4_23.
(17) Virmani, A.; Walavalkar, M. P.; Sharma, A.; Sengupta, S.; Saha, A.; Kumar, A. Kinetic Studies of the Gas Phase Reaction of 1,2-Propylene Oxide with the OH Radical over a Temperature Range of 261–335 K. *Atmos. Environ.* **2020**, *237*, 117709. https://doi.org/10.1016/j.atmosenv.2020.117709.
(18) Mellouki, A.; Téton, S.; Laverdet, G.; Quilgars, A.; Le Bras, G. Kinetic Studies of OH Reactions with H_2O_2 , C_3H_8 and CH_4 Using the Pulsed Laser Photolysis-Laser Induced Fluorescence Method. *J. Chim. Phys.* **1994**, *91*, 473–487. https://doi.org/10.1051/jcp/1994910473.
(19) Ren, Y.; Cai, M.; Daële, V.; Mellouki, A. Rate Coefficients for the Reactions of OH Radical and Ozone with a Series of Unsaturated Esters. *Atmos. Environ.* **2019**, *200*, 243–253. https://doi.org/10.1016/j.atmosenv.2018.12.017.
(20) McGillen, M. R.; Baasandorj, M.; Burkholder, J. B. Gas-Phase Rate Coefficients for the OH + *n* -, *i* -, *s* -, and *t* -Butanol Reactions Measured Between 220 and 380 K: Non-Arrhenius Behavior and Site-Specific Reactivity. *J. Phys. Chem. A* **2013**, *117* (22), 4636–4656. https://doi.org/10.1021/jp402702u.
(21) McGillen, M. R.; Bernard, F.; Fleming, E. L.; Burkholder, J. B. HCFC-133a (CF_3CH_2Cl): OH Rate Coefficient, UV and Infrared Absorption Spectra, and Atmospheric Implications. *Geophys. Res. Lett.* **2015**, *42* (14), 6098–6105. https://doi.org/10.1002/2015GL064939.
(22) Bedjanian, Y. Temperature-Dependent Rate Constant for the Reaction of Hydroxyl Radical with 3-Hydroxy-3-Methyl-2-Butanone. *J. Phys. Chem. A* **2019**, *123* (48), 10446–10453. https://doi.org/10.1021/acs.jpca.9b08714.
(23) Morin, J.; Romanias, M. N.; Bedjanian, Y. Experimental Study of the Reactions of OH Radicals with Propane, *n*-Pentane, and *n*-Heptane over a Wide Temperature Range. *Int. J. Chem. Kinet.* **2015**, *47* (10), 629–637. https://doi.org/10.1002/kin.20936.
(24) Bedjanian, Y.; Le Bras, G.; Poulet, G. Kinetic Study of OH + OH and OD + OD Reactions. *J. Phys. Chem. A* **1999**, *103* (35), 7017–7025. https://doi.org/10.1021/jp991146r.
(25) Zhang, X.; Sangwan, M.; Yan, C.; Koshlyakov, P. V.; Chesnokov, E. N.; Bedjanian, Y.; Krasnoperov, L. N. Disproportionation Channel of the Self-Reaction of Hydroxyl Radical, OH + OH → H_2O + O, Revisited. *J. Phys. Chem. A* **2020**, *124* (20), 3993–4005. https://doi.org/10.1021/acs.jpca.0c00624.

(26) Bedjanian, Y.; Kalyan, C. Rate Constants of the Reactions of O(^{3}P) Atoms with Br_2 and NO_2 over the Temperature Range 220-950 K. *Int. J. Chem. Kinet.* **2019**, *51* (7), 476–483. https://doi.org/10.1002/kin.21270.
(27) Burkholder, J. B.; Abbatt, J. *Chemical Kinetics and Photochemical Data for Use in Atmospheric Studies: Evaluation Number 19*.
(28) Bernard, F.; Eyglunent, G.; Daële, V.; Mellouki, A. Kinetics and Products of Gas-Phase Reactions of Ozone with Methyl Methacrylate, Methyl Acrylate, and Ethyl Acrylate. *J. Phys. Chem. A* **2010**, *114* (32), 8376–8383. https://doi.org/10.1021/jp104451v.
(29) Bernard, F.; Magneron, I.; Eyglunent, G.; Daële, V.; Wallington, T. J.; Hurley, M. D.; Mellouki, A. Atmospheric Chemistry of Benzyl Alcohol: Kinetics and Mechanism of Reaction with OH Radicals. *Environ. Sci. Technol.* **2013**, *47* (7), 3182–3189. https://doi.org/10.1021/es304600z.
(30) Zhou, L.; Ravishankara, A. R.; Brown, S. S.; Idir, M.; Zarzana, K. J.; Daële, V.; Mellouki, A. Kinetics of the Reactions of NO_3 Radical with Methacrylate Esters. *J. Phys. Chem. A* **2017**, *121* (23), 4464–4474. https://doi.org/10.1021/acs.jpca.7b02332.
(31) Müller, M.; Piel, F.; Gutmann, R.; Sulzer, P.; Hartungen, E.; Wisthaler, A. A Novel Method for Producing NH_4^+ Reagent Ions in the Hollow Cathode Glow Discharge Ion Source of PTR-MS Instruments. *Int. J. Mass Spectrom.* **2020**, *447*, 116254. https://doi.org/10.1016/j.ijms.2019.116254.
(32) Kaufman, F. Kinetics of Elementary Radical Reactions in the Gas Phase. *J. Phys. Chem.* **1984**, *88* (21), 4909–4917. https://doi.org/10.1021/j150665a024.
(33) Ivanov, A. V.; Trakhtenberg, S.; Bertram, A. K.; Gershenzon, Y. M.; Molina, M. J. OH, HO_2, and Ozone Gaseous Diffusion Coefficients. *J. Phys. Chem. A* **2007**, *111* (9), 1632–1637. https://doi.org/10.1021/jp066558w.
(34) Wallington, T. J.; Dagaut, P.; Liu, R.; Kurylo, M. J. The Gas Phase Reactions of Hydroxyl Radicals with a Series of Esters over the Temperature Range 240-440 K. *Int. J. Chem. Kinet.* **1988**, *20* (2), 177–186. https://doi.org/10.1002/kin.550200210.
(35) Heard, D. E. Rapid Acceleration of Hydrogen Atom Abstraction Reactions of OH at Very Low Temperatures through Weakly Bound Complexes and Tunneling. *Acc. Chem. Res.* **2018**, *51* (11), 2620–2627. https://doi.org/10.1021/acs.accounts.8b00304.
(36) Smith, I. W. M.; Ravishankara, A. R. Role of Hydrogen-Bonded Intermediates in the Bimolecular Reactions of the Hydroxyl Radical. *J. Phys. Chem. A* **2002**, *106* (19), 4798–4807. https://doi.org/10.1021/jp014234w.
(37) Mendes, J.; Zhou, C.-W.; Curran, H. J. Theoretical Chemical Kinetic Study of the H-Atom Abstraction Reactions from Aldehydes and Acids by $\dot{H}$ Atoms and $\dot{O}H$, $H\dot{O}_2$, and $\dot{C}H_3$ Radicals. *J. Phys. Chem. A* **2014**, *118* (51), 12089–12104. https://doi.org/10.1021/jp5072814.
(38) Khamaganov, V. G.; Bui, V. X.; Carl, S. A.; Peeters, J. Absolute Rate Coefficient of the OH + $CH_3C(O)OH$ Reaction at T = 287−802 K. The Two Faces of Pre-Reactive H-Bonding. *J. Phys. Chem. A* **2006**, *110* (47), 12852–12859. https://doi.org/10.1021/jp064922l.
(39) Zhou, C.-W.; Simmie, J. M.; Curran, H. J. Rate Constants for Hydrogen Abstraction by $H\dot{O}_2$ from N-Butanol. *Int. J. Chem. Kinet.* **2012**, *44* (3), 155–164. https://doi.org/10.1002/kin.20708.
(40) Cavalli, F.; Geiger, H.; Barnes, I.; Becker, K. H. FTIR Kinetic, Product, and Modeling Study of the OH-Initiated Oxidation of 1-Butanol in Air. *Environ. Sci. Technol.* **2002**, *36* (6), 1263–1270. https://doi.org/10.1021/es010220s.

(41) Shannon, R. J.; Blitz, M. A.; Goddard, A.; Heard, D. E. Accelerated Chemistry in the Reaction between the Hydroxyl Radical and Methanol at Interstellar Temperatures Facilitated by Tunnelling. *Nat. Chem.* **2013**, *5* (9), 745–749. https://doi.org/10.1038/nchem.1692.

(42) St. John, P. C.; Guan, Y.; Kim, Y.; Kim, S.; Paton, R. S. Prediction of Organic Homolytic Bond Dissociation Enthalpies at near Chemical Accuracy with Sub-Second Computational Cost. *Nat. Commun.* **2020**, *11* (1), 2328. https://doi.org/10.1038/s41467-020-16201-z.

(43) St. John, P. C.; Guan, Y.; Kim, Y.; Etz, B. D.; Kim, S.; Paton, R. S. Quantum Chemical Calculations for over 200,000 Organic Radical Species and 40,000 Associated Closed-Shell Molecules. *Sci. Data* **2020**, *7* (1), 244. https://doi.org/10.1038/s41597-020-00588-x.

(44) Seakins, P. W.; Pilling, M. J.; Niiranen, J. T.; Gutman, D.; Krasnoperov, L. N. Kinetics and Thermochemistry of R + Hydrogen Bromide .Dblarw. RH + Bromine Atom Reactions: Determinations of the Heat of Formation of Ethyl, Isopropyl, Sec-Butyl and Tert-Butyl Radicals. J. Phys. Chem. **1992**, 96 (24), 9847–9855. https://doi.org/10.1021/j100203a050.

(45) Krasnoperov, L. N.; Peng, J.; Marshall, P. Modified Transition State Theory and Negative Apparent Activation Energies of Simple Metathesis Reactions: Application to the Reaction $CH_3 + HBr \rightarrow CH_4 + Br$ [†]. *J. Phys. Chem. A* **2006**, *110* (9), 3110–3120. https://doi.org/10.1021/jp054435q.

(46) Gao, Y.; Alecu, I. M.; Hsieh, P.-C.; Morgan, B. P.; Marshall, P.; Krasnoperov, L. N. Thermochemistry Is Not a Lower Bound to the Activation Energy of Endothermic Reactions: A Kinetic Study of the Gas-Phase Reaction of Atomic Chlorine with Ammonia [†]. *J. Phys. Chem. A* **2006**, *110* (21), 6844–6850. https://doi.org/10.1021/jp056406l.

(47) McGillen, M. R.; Tyndall, G. S.; Orlando, J. J.; Pimentel, A. S.; Medeiros, D. J.; Burkholder, J. B. Experimentally Determined Site-Specific Reactivity of the Gas-Phase OH and Cl + *i* -Butanol Reactions Between 251 and 340 K. *J. Phys. Chem. A* **2016**, *120* (50), 9968–9981. https://doi.org/10.1021/acs.jpca.6b09266.

(48) Jacobs, M. I.; Darer, A. I.; Elrod, M. J. Rate Constants and Products of the OH Reaction with Isoprene-Derived Epoxides. *Environ. Sci. Technol.* **2013**, *47* (22), 12868–12876. https://doi.org/10.1021/es403340g.

(49) Bates, K. H.; Crounse, J. D.; St. Clair, J. M.; Bennett, N. B.; Nguyen, T. B.; Seinfeld, J. H.; Stoltz, B. M.; Wennberg, P. O. Gas Phase Production and Loss of Isoprene Epoxydiols. *J. Phys. Chem. A* **2014**, *118* (7), 1237–1246. https://doi.org/10.1021/jp4107958.

For TOC only

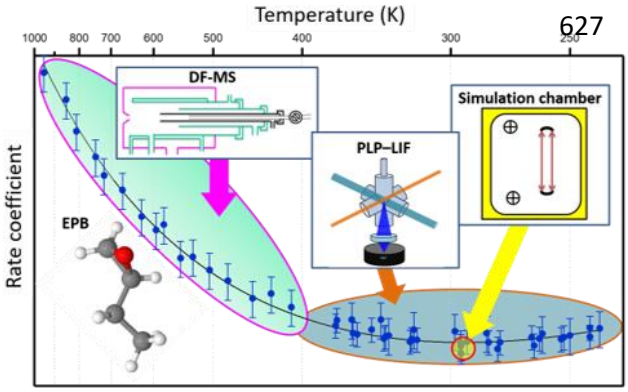
Temperature (K)
1000
800
700
600
500
400
300
200
Rate coefficient
DF-MS
PLP–LIF
Simulation chamber
EPB